AUTOMATIC SEGMENTATION OF EMBRYONIC HEART IN TIME-LAPSE FLUORESCENCE MICROSCOPY IMAGE SEQUENCES

P. Krämer, F. Boto[1], D. Wald, F.Bessy, C. Paloc
Vicomtech, Paseo de Mikeletegi 57, 20009 Donostia, San Sebastián, Spain

C. Callol[2], A. Letamendia, I. Ibarbia, O. Holgado, J. M. Virto
Biobide, Paseo de Mikeletegi 58, 20009 Donostia, San Sebastián, Spain

Keywords: Segmentation, Fluorescent microscopy images, Embryonic heart.

Abstract: Embryos of animal models are becoming widely used to study cardiac development and genetics. However, the analysis of the embryonic heart is still mostly done manually. This is a very laborious and expensive task as each embryo has to be inspected visually by a biologist. We therefore propose to automatically segment the embryonic heart from high-speed fluorescence microscopy image sequences, allowing morphological and functional quantitative features of cardiac activity to be extracted. Several methods are presented and compared within a large range of images, varying in quality, acquisition parameters, and embryos position. Although manual control and visual assessment would still be necessary, the best of our methods has the potential to drastically reduce biologist workload by automating manual segmentation.

1 INTRODUCTION

Model organisms have become more and more important for the study of vertebrate development. Due to its prolific reproduction and the external development of the transparent embryo, they are prime models for genetic and developmental studies, as well as research in toxicology and genomics. While genetically more distant from humans, the vertebrate models nevertheless have comparable organs and tissues, such as heart, kidney, pancreas, bones, and cartilage.

During the last years tremendous advances in imaging system have been made allowing the acquisition of high-resolution images of embryos. Anyhow, the processing of such images is still a challenge (Vermot et al., 2008). To date, only little work has been presented addressing the analysis of embryo models images (Fink et al., 2009; Luengo-Oroz et al., 2007; Liebling et al., 2006). For instance (Liebling et al., 2006) presents a method to acquire, reconstruct and analyze 3D images of the zebrafish heart. The reconstruction of the volume is based on a semi-automatic segmentation procedure and requires the help of the user. Fink et al., 2009 propose a method for detection and quantification of heartbeat parameters in Drosophilia deriving a signal from the images, avoiding segmentation.

In case of studies of cardiac development, a segmentation of the heart provides additional information for its quantification. Therefore, we present several approaches to automatically extract its shape and each chamber from image sequence. In our experiment, transgenic embryos expressing fluorescent protein in the myocardium were placed under light microscopy allowing to capture fluorescent images of the heart at video rate. In particular, we are interested in segmenting the heart of zebrafish embryos after two days of post-fertilization (2 dpf). In early stages of the zebrafish development the primitive heart begins a simple linear tube. This structure gradually forms into two chambers, a ventricle and an atrium. At 2 dpf the heart tube is already partitioned into atrium and ventricle as depicted in Figure 1. They are separated by a constriction which will later form the valve. At this stage the heart is already beating. More information on zebrafish heart anatomy can be found

Krämer P., Boto F., Wald D., Bessy F., Paloc C., Callol C., Letamendia A., Ibarbia I., Holgado O. and Virto J. (2010).
AUTOMATIC SEGMENTATION OF EMBRYONIC HEART IN TIME-LAPSE FLUORESCENCE MICROSCOPY IMAGE SEQUENCES.
In *Proceedings of the Third International Conference on Bio-inspired Systems and Signal Processing*, pages 121-126
DOI: 10.5220/0002342501210126

in (Hu et al., 2000).

The remainder is organized as follows: In section 2 we present several approaches to segment the zebrafish heart and in section 3 two methods to identify the chambers. In section 4 we show some results and compare the segmentation methods respectively for the heart and its chambers. We give a conclusion of our work and outline future research in section 5.

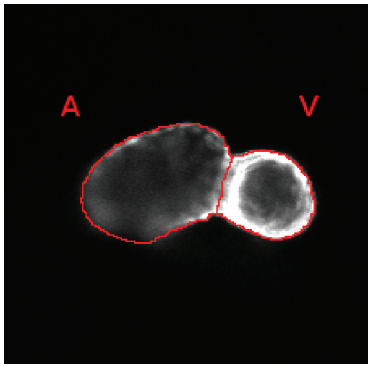

Figure 1: The 2 dpf zebrafish heart already consists of two chambers: the atrium (A) and ventricle (V).

2 SEGMENTATION OF THE ZEBRAFISH HEART

In this section we outline different approaches to segment the shape of the zebrafish heart. For the methods of subsection 2.3, 2.4, 2.5, we cast the images to 8-bit grey level images and stretch the grey level range into [0,255].

2.1 Adaptive Binarization

This method is based on the assumption that the image of the heart consists of three brightness levels such as illustrated in Figure 2: one corresponding to the background and two corresponding to the fluorescent heart where strong contracted regions appear brighter due to a higher concentration of fluorescent cells.

For pre-processing, we smooth image using a Gaussian filter to remove noise. Then, the region of the heart with highest brightness is segmented by first applying a Contrast-Limited Adaptive Histogram Equalization (CLAHE) (Zuiderveld, 1994) using a uniform transfer function and then the automatic threshold method from Otsu (Otsu, 1979). In order to segment the second, less brighter region of the heart, we exclude the previous segmented

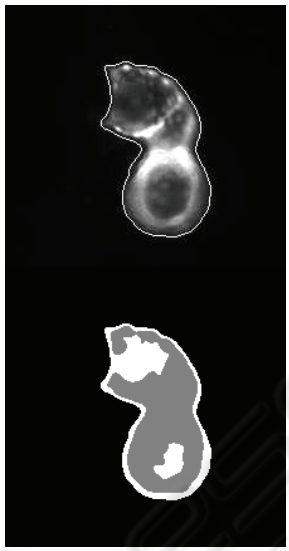

Figure 2: The image of fluorescent heart consists of three brightness levels: one corresponding to the background and two to the heart.

region and apply CLAHE and Otsu again. The final segmentation is obtained by combining both segmentation results. Postprocessing includes the filling of holes which can appear inside in the shape.

2.2 Clustering

This method is based on unsupervised classification in order to distinguish between object and background pixels. First, each pixel is characterized by the mean luminance value of the 3×3 mask centered at the pixel. A unidimensional feature space results. Then, we use a k-means classifier (k=3) in order to separate the pixels into three clusters. This method relies like the previous one on the assumption than that there are three different brightness levels. The cluster to which belongs the pixel at position (0,0) is then defined as the background and others as the region of the heart. Similarly than above, we apply hole filling as postprocessing. For more information on k-means clustering can be found in (Bishop, 2007).

2.3 Voronoi-based Segmentation

The Voronoi segmentation (Imelinska et al., 0002) is based on repeatedly dividing an image into regions using Voronoi diagram and classifying the regions as either inside or outside the target based on classification statistics, and then break up the regions on the boundary between the two classifications into smaller regions and repeat the

classification and subdivision on the new set of regions. The classification statistics can be obtained from an image prior which is a binary image of preliminary segmentation.

In order to compute the image prior, we apply first a bilateral filter to smooth the image while preserving edges. Afterwards, the gradient magnitude is computed using a recursive Gaussian filter and Sigmoid filter to map the intensity range into [0,255]. Then a threshold is applied to the gradient magnitude to obtain a binary mask. As the binary mask may contain holes, we apply a morphological closing operation and fill the holes to complete the object's shape. Then the main region of the heart is isolated from noise in the binary image by a region growing algorithm to the binary with the brightest pixel in the image as seed point. Typically, the brightest pixel in the gray-level image belongs to the region of the heart. After the Voronoi segmentation we apply again morphological closing, hole filling, isolation of the main region, and morphological erosion to smooth the contours.

2.4 Level Set

The idea of this method is similar to the previous one. First a pre-segmentation accomplished which is then refined, but here we use the level set approach (Li et al., 2005) for refinement. We choose this method because of its fast performance.

The method starts with a morphological reconstruction to suppress structures that are lighter than their surroundings and that are connected to the image border. Then, edges are detected using the Canny edge detector. Dilation, hole filling, and erosion are applied to the contour image. The biggest region is considered as the region of the heart while the others are considered as noise. We complete the form by applying again dilation and hole filling.

A Gaussian filter is applied to smooth the original grey level image for noise removal. Then we apply the level set method (Li et al., 2005) with contours of the binary mask as initialization. We chose the edge indicator function 1/(1+g) as suggested by the author where g is the gradient magnitude of the Gaussian filtered grey level image.

2.5 Watershed

This approach is different to the previous one as it does not rely on a pre-segmentation by binarization. It is based on Watershed segmentation.

First the border structures are supressed by morphological reconstruction. This is followed by a strong low-pass filtering (Gaussian filter) in a morphological reconstruction by erosion using the inverse of morphological gradient. This attenuates unwanted portions of the signal while maintaining the signal intensity as the Watershed method is known to oversegment the image. Afterwards, a small threshold is applied to set the background to zero and the image intensity is adjusted so that such that 1% of data is saturated at low and high intensities. We apply to this gradient magnitude the watershed segmentation. An oversegmented image may result with typically one region belonging to the background and several regions belonging to the heart. The latter ones are joined to form the region of the heart.

3 IDENTIFICATION OF THE CHAMBERS

The objective is now to divide the heart into the chambers based on the results of the methods presented in the previous section.

3.1 Convexity Defects

The method assumes that there is a constriction between the two chambers (see Figure 1) causing two convex points in the contour of the heart's shape. Therefore, we compute the convexity defects of the contour using its convex hull. Generally more than two convexity defects are found due to irregularities in the contour caused by the segmentation as depicted in Figure 3. Moreover, we assume that the convexity defects denoting the constriction between the chambers are parallel. Thus, we choose the four most important convexity defects, i.e. the four points with the highest distance from the convex hull, and compute the angle for each pair as:

$$\theta = arccos\left(\frac{v_1 \cdot v_2}{|v_1||v_2|}\right) \quad (1)$$

where v1,v2 are respectively the vectors between the start and end points of the first and second convexity defects. If the angle is lower than a small threshold, then the pair of convexity defects is considered as a possible candidate for the constriction, otherwise it is rejected. Finally, we choose the pair with the highest mean distance as the points of the constriction from the remaining. We compute the straight line interpolating the points which separates both chambers. As there is often a high variation of the straight line along the image sequence, we correct it by Double Exponential Smoothing-Based

Prediction (DESP) (LaViola Jr., 2003) using the results of the previous images.

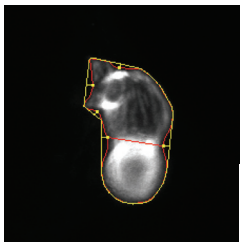

Figure 3: The segmented heart (inside line) and the convex hull (outside line) with convexity defects of the shape (points).

3.2 Watershed

This method is based on the results of the Watershed segmentation of subsection 2.5. The general idea is to divide the segmented shape into the two chambers by applying a second watershed segmentation. Therefore, the background is masked out and a watershed segmentation is applied in this area after a strong low-pass filtering. If two regions result, then they correspond to a rough identification of two chambers. Otherwise the regions have to be joined until only two regions remain. Therefore, we use the chamber identification of the previous image. We compute the intersection of a region in the current image with the identified chambers of the previous image. Then, the region is identified to belong to the chamber where the intersection is maximal. It can happen that only one region is obtained by the Watershed segmentation. Then, the segmentation of the previous image is used for further processing of the current image.

This chamber identification is very rough whereas the outline is not coincident with that one of subsection 2.5 as can be seen in Figure 4. Thus unassigned pixels remain. In order to assign them to one of the chambers, an Euclidean distance transform is computed for each chamber. Then, the non-assigned pixels of the segmentation are joined with the chamber for which the distance transform is smaller.

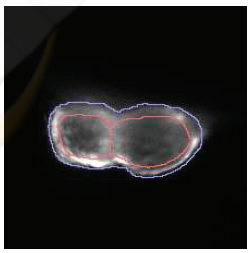

Figure 4: The Watershed segmentation (outline line) and the first rough identification of the chambers (inside line).

4 RESULTS AND DISCUSSION

In this section, we show and discuss the results obtained with the methods presented above. First, we compare the algorithms for segmenting the shape of the heart from section 2 using an accuracy measure. Then, we evaluate visually the results of chamber segmentation algorithms from section 3.

4.1 Comparison of Segmentation Algorithms

Several methods exist to measure the performance of segmentation algorithms (Zhang et al., 2008; Sezgin and Sankur, 2004). Here, we choose to compare the segmented images with ground truth images which were obtained by manual segmentation.

We used the Jaccard coefficient (Cox and Cox, 2001; Ge et al., 2007) as performance measure for each segmentation method. This coefficient measures the coincidence between the segmentation result R and the ground truth A. Then, the segmentation accuracy is measured as:

$$P(R,A) = \frac{|R \cap A|}{|R \cup A|} = \frac{|R \cap A|}{|R| + |A| - |R \cap A|} \quad (2)$$

with $|\cdot|$ as the number of pixels of the given region. The nominator $|R \cap A|$ means how much of the object has been detected while the denominator $|R \cup A|$ is a normalization factor to scale the accuracy measure into the range of [0,1]. Likewise pixels falsely detected as belonging to the object (false positives) are penalized by the normalization factor. Thus, this accuracy measure is insensitive to small variations in the ground truth construction and incorporates both, false positives and negatives, in one unified function (Ge et al., 2007).

In our experiments we used 26 image sequences with a resolution of 124×124 pixels. For each image sequence we segmented the first 20 images with the above presented methods and compared them with a ground truth segmentation. We only chose sequences with fair image quality for evaluation as otherwise the accuracy of the manual segmentation is too subjective (Figure 5).

The results of Jaccard coefficient for each sequence are presented in Table 1. The Voronoi-based and both thresholding methods outperform the watershed and level set methods. A visual inspection of the segmentation results reveals similar results.

Table 1: Mean accuracy for the segmentation algorithms.

Method	Mean accuracy	Standard deviation	Max accuracy	Min accuracy
Adaptive binarization	0.870	0.052	0.946	0.725
Clustering	0.876	0.057	0.954	0.759
Voronoi segmentation	0.890	0.046	0.937	0.769
Level set	0.850	0.062	0.965	0.724
Watershed	0.856	0.044	0.896	0.717

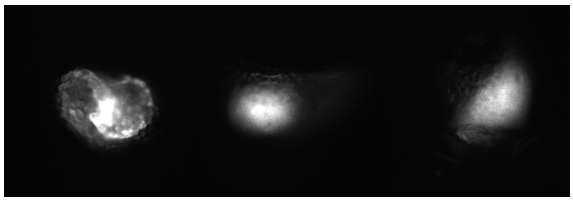

Figure 5: Rejected samples. Overlapping chambers and blurred images.

The level set method gives good results on high contrast edges, but in regions where edges are blurred, the level set does not approach well the shape of the heart resulting in holes in the object shape or a too large shape. Moreover, we found it difficult to determine a common set of parameters suitable for all sequences.

The contours of the watershed method appear very rough and are often too tight. This might be due to the strong low-pass filtering in the post-processing which causes an edge mismatch. Equally a false classification of the regions into background and foreground may cause an inaccurate segmentation.

The Voronoi-based segmentation method reveals the best results in term of accuracy measure. The contours are typically slightly irregular; some postprocessing could be applied to smooth them. In case of low-contrast contours it may behave similar to the level set method. The overall results are quite satisfying.

The adaptive binarization tends to have a slightly larger contour, but approaches well the object shape. This might cause the lower accuracy results, but the overall segmentation results are good. Sometimes in case of low-contrast edges the object shape may be incomplete.

The clustering method tends also to larger contours, but slightly tighter than the adaptive binarization method. Therefore, a higher accuracy is achieved. However, in case of low-contrast edges it reveals more often incomplete shapes than the adaptive binarization. Note that the accuracy can vary as the randomized choice of initial cluster may result in slightly different segmentation results.

The computational cost cannot be directly compared as the implementations use different programming languages and libraries (the adaptive binarization, clustering, and Voronoi methods are implemented in C++ using respectively OpenCV, OpenCV and Torch, and ITK; the level set and watershed methods are implemented in Matlab). However, the execution time for each image is reasonable and estimated at about one second independently of the method.

4.2 Chamber Identification

In this section, we present some results of the convexity defects and watershed methods used to divide the heart into two chambers. The convexity defects method was evaluated only in combination with the adaptive binarization and clustering methods, as they present good segmentation results (see previous section).

For evaluation we used only 24 out of the 26 sequences from above, because in two other ones the chambers are superimposed (Figure 5). Such cases are not taken in consideration in current developments, and we therefore chose to discard those sequences. 480 images were then segmented using each of the described method, and visually inspected to evaluate whether the heart was correctly divided. Our results are shown in Table 2, where the best result is obtained for the adaptive binarization method.

Table 2: The ratio of correct chamber identification per image for the chamber identification algorithms.

Method	Ratio
Adaptive binarization + convexitydefects	0.704
Clustering + convexity defects	0.577
Watershed	0.456

5 CONCLUSIONS AND FUTURE WORK

We presented a first attempt of automatically segmenting the shape and the chambers of the

zebrafish embryonic heart from time-lapse fluorescence microscopy image sequences.

For segmenting the shape of the heart, the Voronoi-based and both thresholding methods outperform the watershed and level set methods. The Voronoi-based segmentation gives the best results in terms of the accuracy measure, as thresholding methods tend to fail in cases of low-contrast edges.

The watershed segmentation results in quite rough contours. Anyhow, it is an interesting approach as it is the basis for chamber identification. The results of the level set method are not satisfying. For chamber identification the adaptive binarization method in combination with the detection of convexity defects outperforms clearly the other methods.

Besides segmentation in order to extract morphological information, we are also working on other processing methods to extract cardiac function metrics from image sequence. Such methods are able to provide additional information for cardiac development study with very high accuracy.

REFERENCES

Bishop, C.M. (2007). *Pattern Recognition and Machine Learning*. (Information Science and Statistics). Springer.

Cox, T. and Cox, M. (2001). *Multidimensional Scaling* (2nd ed.). Chapman & Hall/CRC.

Fink, M., Callol-Massot, C., Chu, A., Ruiz-Lozano, P., Belmonte, J. C., Giles, W., Bodmer, R., and Ocorr, K. (2009). A new method for detection and quantification of heartbeat parameters in drosophila, zebrafish, and embryonic mouse hearts. *BioTechniques*, 46(2), 101–113.

Ge, F., Wang, S., and Liu, T. (2007). New benchmark for image segmentation evaluation. *Journal of Electronic Imaging*, 16(3):033011.

Hu, N., Sedmera, D., Yost, H., and Clark, E. (2000). Structure and function of the developing zebrafish heart. *The Anatomical Record*, 260(2), 148–157.

Imelinska, C., Downes, M., and Yuan, W. (2002). Semi-automated color segmentation of anatomical tissue. *Computerized Medical Imaging and Graphics*, 24, 173–180.

LaViola Jr., J. (2003). Double exponential smoothing: An alternative to kalman filter-based predictive tracking. *In Immersive Projection Technology and Virtual Environments*, 199–206.

Li, C., Xu, C., Gui, C., and Fox, M. (2005). Level set evolution without re-initialization: A new variational formulation. *CVPR*, 1, 430–436. IEEE.

Liebling, M., Forouhar, A., Wolleschensky, R., Zimmermann, B., Ankerhold, R., Fraser, S., Gharib, M., and Dickinson, M. E. (2006). Rapid three-dimensional imaging and analysis of the beating embryonic heart reveals functional changes during development. *Developmental Dynamics*, 235(11), 2940–2948.

Luengo-Oroz, M., Faure, E., Lombardot, B., Sance, R., Bourgine, P., Peyri´eras, N., and Santos, A. (2007). Twister segment morphological filtering. A new method for live zebrafish embryos confocal images processing. *ICIP*, 253–256. IEEE.

Otsu, N. (1979). A threshold selection method from graylevel histograms. *IEEE Trans. on Systems, Man and Cybernetics*, 1(9), 62–69.

Sezgin, M. and Sankur, B. (2004). Survey over image thresholding techniques and quantitative performance evaluation. *Journal of Electronic Imaging*, 13(1), 146–168.

Vermot, J., Fraser, S., and Liebling, M. (2008). Fast fluorescence microscopy for imaging the dynamics of embryonic development. *HFSP Journal*, 2(3), 143–155.

Zhang, H., Fritts, J., and Goldman, S. (2008). Image segmentation evaluation: A survey of unsupervised methods. *Computer Vision and Image Understanding*, 110(2), 260–280.

Zuiderveld, K. (1994). *Graphics Gems IV*, chapter Contrast Limited Adaptive Histogram Equalization, pages 474–485. Academic Press.